

Article

## Improving the Ethanol Oxidation Activity of Pt-Mn Alloys through the Use of Additives during Deposition

Mohammadreza Zamanzad Ghavidel and E. Bradley Easton \*

Faculty of Science, University of Ontario Institute of Technology, 2000 Simcoe Street North, Oshawa, ON L1H 7K4, Canada; E-Mail: mohammadreza.ghavidel@uoit.ca

\* Author to whom correspondence should be addressed; E-Mail: brad.easton@uoit.ca; Tel.: +1-905-721-8668 (ext. 2936); Fax: +1-905-721-3304.

Academic Editor: Minhua Shao

Received: 15 May 2015 / Accepted: 16 June 2015 / Published: 25 June 2015

---

**Abstract:** In this work, sodium citrate (SC) was used as an additive to control the particle size and dispersion of Pt-Mn alloy nanoparticles deposited on a carbon support. SC was chosen, since it was the only additive tested that did not prevent Mn from co-depositing with Pt. The influence of solution pH during deposition and post-deposition heat treatment on the physical and electrochemical properties of the Pt-Mn alloy was examined. It was determined that careful control over pH is required, since above a pH of four, metal deposition was suppressed. Below pH 4, the presence of sodium citrate reduced the particle size and improved the particle dispersion. This also resulted in larger electrochemically-active surface areas and greater activity towards the ethanol oxidation reaction (EOR). Heat treatment of catalysts prepared using the SC additive led to a significant enhancement in EOR activity, eclipsing the highest activity of our best Pt-Mn/C prepared in the absence of SC. XRD studies verified the formation of the Pt-Mn intermetallic phase upon heat treatment. Furthermore, transmission electron microscopy studies revealed that catalysts prepared using the SC additive were more resistant to particle size growth during heat treatment.

**Keywords:** Pt-Mn alloy; additive; heat treatment; ethanol oxidation; catalysts; PEM fuel cell; direct alcohol fuel cell

---

## 1. Introduction

Problems associated with the costs and efficiency of fuel cells are a great barrier for industrial and consumer applications [1–4]. Direct alcohol fuel cells (DAFCs) are one of the most promising candidates for portable power applications in electronic devices and vehicles [4]. The cost and performance of the DAFCs are mainly controlled by the catalysts used at each electrode. Pt is the most commonly utilized electrocatalyst, which is quite expensive [3]. Furthermore, strongly adsorbing species, such as CO, which are formed during the alcohol oxidation process on pure Pt particles, result in severe activity and efficiency losses [4,5]. The development of Pt alloy catalysts offers the potential of greater tolerance to poisoning and significant cost reduction. Likewise, decreasing Pt alloy particle sizes and improving particle dispersion can further increase performance [3], although there is some debate about the effects of particle size on catalytic activity [6,7].

The Pt-Mn alloy system has recently been identified by our group as having enhanced activity towards the ethanol oxidation reaction (EOR) [8,9]. Alloy formation was confirmed with X-ray powder diffraction (XRD) analysis, and the most active alloys contained less than 25 at% Pt, which is beneficial from a cost standpoint. The results showed that the presence of Mn affects both particle size and the intrinsic activity of the catalysts. Further study by the authors also showed that post-heat treatment had a great impact on the activity of the Pt-Mn alloys, and the main reason for enhancing the EOR activity was the formation of Pt-Mn intermetallic phase [10]. However, particle size growth during heat treatment was an unwanted consequence of heat treatment. Sintering can happen by the migration and coalescence of the catalyst particles or by evaporation and condensation of the atoms from small crystallites [11]. While the benefits of thermally treating alloy nanoparticles out-weighed any activity losses that may occur due to particle size growth, it would be desirable to find a way to produce smaller particles with better dispersion that are resistant to particle growth during heat treatment.

Common strategies used to deposit small and well-dispersed metal nanoparticles on carbon include functionalization of the support [12], using the polyol [13] or microemulsion [14,15] deposition methods [11,16] employing surfactants [17,18], which are significant strategies to improve particle dispersion and to reduce particle sizes. It has been shown that oxygenated surface groups on the carbon support can enhance the dispersion and the stability of Pt/C catalysts [11]. However, oxygen containing groups can be reduced during the reduction step, which can result in the redistribution of platinum particles and less favorable Pt dispersion [11]. Studies have shown that nitrogen functionalization on carbon can improve cathode performance [11,19]. While Dinotto and Negro [20,21] have produced some carbon nitride-based electrocatalysts at lower temperatures, nitrogen groups are more commonly introduced via high temperature processes that can also alter the porosity and microstructure of the support [11]. Unfortunately, the efforts in our group to produce Pt-Mn alloys from polyol and microemulsion methods were not successful because of very negative reduction potential for Mn ions in these solutions, which prevented Mn co-deposition [22].

Several studies [17,18,23,24] have shown that adding surfactants reduces the particle sizes of Pt and Pt alloys nanoparticles and also improves their dispersion on the support [25]. Sodium citrate (SC) is a common surfactant used in both aqueous and organic solutions by numerous researchers to produce Pt [18], Pt-Au [26], PtRuIr [27] and Pt-Co [28] nano-particles that were small (2–6 nm) with a narrow

size distribution. However, to the best of our knowledge, SC has not been used to prepare Pt-Mn alloys [18,26–28].

In this paper, the effect of sodium citrate on particle size, dispersion, structure and EOR activity of Pt-Mn was investigated. In addition, the influence of solution pH and heat treatment on the crystalline structure, the uniformity of alloyed phases and the activity of the catalysts has been examined.

## 2. Results and Discussion

### 2.1. Material Characterization

Citric acid is a polyprotic acid, with pKa values of 3.14, 4.76 and 6.40 for each acid site. As such, the charge on SC will be influenced by solution pH, which can influence both Mn and Pt deposition, as well as the resulting particle sizes. Our preliminary studies showed that pH had an impact on Mn and Pt deposition. When the solution pH was above three, the metal loading and, as a consequence, the electrochemical activity of the sample dropped, and different trends were seen from sample to sample at higher pHs (Figure S1). We believe that at higher pHs, there is a stronger interaction between the citrate ions and  $Mn^{2+}$  ions in the precursor solution, which prevents them from deposition. Therefore, in this paper, all of the samples have been produced at pH 3.

Table 1 contains the post-chemical reduction composition of the Pt-Mn catalyst samples and the residual solutions, which were determined by inductively-coupled plasma optical emission spectroscopy (ICP-OES). Catalysts were prepared using SC to metal weight ratios of 1:1, 2:1 and 3:1, which are hereafter referred to as 1X, 2X and 3X, respectively. These results showed that the Pt-Mn alloys were produced with a molar ratio close to the calculated values. By adding SC, a small increase in the amount of metal ions in the residual solution was observed, especially the Pt content.

**Table 1.** Composition of the samples and concentration of Pt and Mn in filtrated solution, which was measured by ICP, along with grain size measured by TEM.

Samples	Alloy molar ratios measured by ICP		Ions concentration in filtrated solution by ICP		Grain size measured by TEM (nm)
	Pt (%)	Mn (%)	Pt (ppm)	Mn (ppm)	
Pt <sub>0.25</sub> Mn <sub>0.75</sub>	22.18	77.82	nil	nil	4.5
Pt <sub>0.25</sub> Mn <sub>0.75</sub> -1X	20.30	79.70	0.49	nil	2.6
Pt <sub>0.25</sub> Mn <sub>0.75</sub> -2X	20.56	79.44	8.23	nil	2.8
Pt <sub>0.25</sub> Mn <sub>0.75</sub> -3X	21.94	78.06	11.70	0.20	2.9
Pt <sub>0.25</sub> Mn <sub>0.75</sub> -2X-500-1 h	-	-	-	-	5.7
Pt <sub>0.25</sub> Mn <sub>0.75</sub> -2X-700-1 h	-	-	-	-	5.8
Pt <sub>0.25</sub> Mn <sub>0.75</sub> -2X-875-1 h	-	-	-	-	6.0
Pt <sub>0.25</sub> Mn <sub>0.75</sub> -2X-950-1 h	-	-	-	-	6.6

The thermogravimetry (TG) and derivative thermogravimetry (DTG) of Pt-Mn alloys, which were synthesized on a Vulcan carbon support in the presence and absence of SC, are shown in Figure 1a,b. Five distinctive mass loss regions are observed in Figure 1. The mass loss between 100 °C and 250 °C was attributed to the thermal decomposition of residual, weak carbon functional groups and water evaporation in the powders [29,30]. A second major mass loss began at 300 °C, which was related to the

oxidation of carbon black by the oxygen or the air trapped within the powder particles [30]. The mass loss at 700–800 °C is attributed to the loss of various functionalized groups on the carbon surface and graphitization [29]. The mass loss at 577 and 928 °C, for the sample prepared without additive, and at 460 and 919 °C, for the sample prepared in the presence of SC, was attributed to Mn oxide phase modifications and a reduction in the amount of oxygen [31]. It has been shown that pure MnO<sub>2</sub> is reduced to Mn<sub>2</sub>O<sub>3</sub> at 500 °C and further reduced to Mn<sub>3</sub>O<sub>4</sub> at 900 °C [30]. The source of mass loss observed at ~1076 °C was not identified. However, from the TG and DTG diagrams of the samples prepared with and without SC, it could be concluded that the temperature required for most of the phase transitions was moved to lower temperatures and facilitated by adding SC.

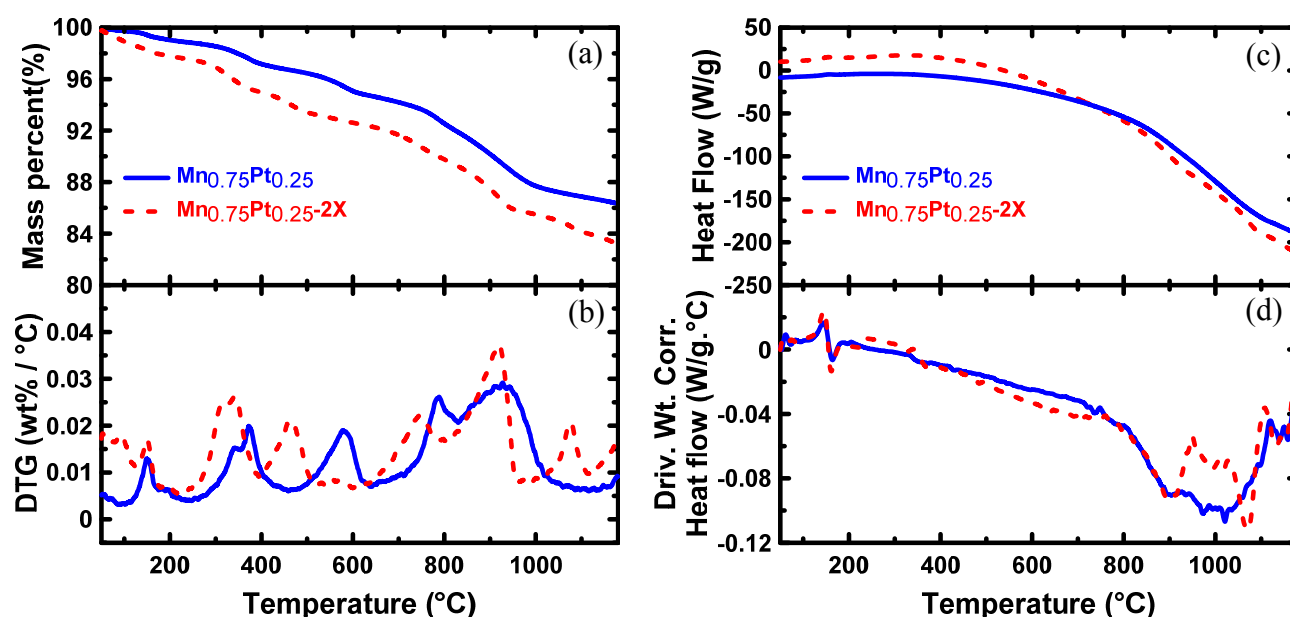


**Figure 1.** (a) TG, (b) DTG, (c) DSC and (d) derivative weight-corrected DSC for Pt-Mn alloys, which were synthesized on Vulcan carbon support in the presence and absence of sodium citrate.

Figure 1b illustrates the DSC curves obtained for Pt-Mn alloys prepared in the presence and absence of SC. Most of the reactions were endothermic, except those related to carbon oxidation at 300–400 °C. The derivative heat flow diagrams from 700–1200 °C showed that the heat flow in the presence of the additive was divided into two separate peaks. The first peak was related to an expected phase transformation from the Pt-Mn phase diagram [32] or Mn oxide phase modifications. The second peak might be attributed to the alloy melting or unknown phase transformation. As catalysts were not prepared at heat treatments above 950 °C, this was not examined in detail. The measured heat between 700–1000 °C (3.97 mW/g) for the Pt-Mn alloy prepared without SC is higher than that measured for the sample synthesized by SC (2.89 mW/g). Therefore, adding SC decreased the heat required for the phase transformation and facilitated the alloying process. Based on the DSC results, heat treatment temperatures of 500, 700, 875 and 950 °C were selected to compare the electrochemical and structural changes of Pt-Mn samples prepared with and without SC.

Figure 2 shows the TGA diagrams and mass loss in air. The mass lost at around 400 °C was due to carbon combustion. The Vulcan carbon ignition was around 600 °C, which was facilitated in the presence

of metal. The data calculated from Figure 2 are presented in Table 2. The results showed that when SC is used, the combustion temperature is reduced by *ca.* 80 °C. This implies that the Pt-alloy particle size was reduced and the particle dispersion was improved. It was previously observed that by increasing Pt loading and available Pt surface area, the combustion temperature of carbon black was decreased because of a higher oxygen and carbon reaction rate [30,33]. Finally, the residual mass above 600 °C indicated that the metal loading in all samples was close to the expected 20 wt%.

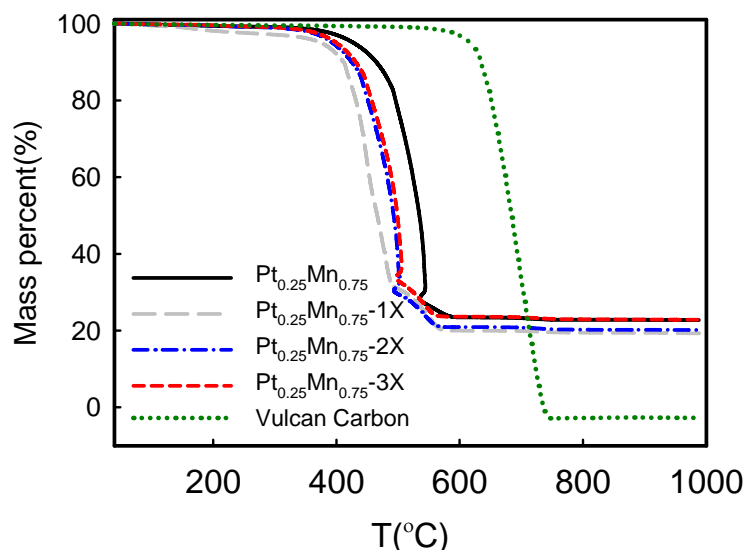


**Figure 2.** The effect of sodium citrate concentration on the weight loss of Pt-Mn alloys, which were synthesized on Vulcan carbon support.

**Table 2.** The metal loading and the Vulcan carbon combustion temperature measured from Figure 2.

Samples	Carbon black combustion Temperature (°C)	Metal loading (wt. %)
Pt <sub>0.25</sub> Mn <sub>0.75</sub>	429.2	22.6
Pt <sub>0.25</sub> Mn <sub>0.75</sub> -1X	348.4	19
Pt <sub>0.25</sub> Mn <sub>0.75</sub> -2X	350.7	20.1
Pt <sub>0.25</sub> Mn <sub>0.75</sub> -3X	359.5	22.8
Vulcan carbon	633.4	-

XRD patterns obtained for Pt-Mn alloy catalysts prepared with varying amounts of SC are shown in Figure 3. We have previously reported that as-deposited catalysts contained a mixed structure of Pt-Mn alloys and non-alloyed phases [10]. Broad peaks indicate that alloy particles with small grain sizes were produced. The broadening of the peaks can also be due to the presence of oxide phases and/or non-uniform alloys. The diffractogram displayed the characteristics of the face-centered cubic (fcc) structure of Pt, and the peaks were shifted to higher angles, indicating the incorporation of Mn in the fcc structure. Additionally, there is a peak at 36.2°, which is likely related to Mn-rich phases. Moreover, it can be concluded that, by adding SC, the peaks became broader, which was the result of the particle size reduction. Increasing the concentration of sodium citrate up to 2X reduced the amount of oxide phases. However, the oxide phases reappeared after the amount of sodium citrate was increased to 3X.

It seems that the optimum amount for the SC concentration is 2X. Therefore, catalysts prepared with a 2X ratio were selected for a more detailed heat-treatment investigation.

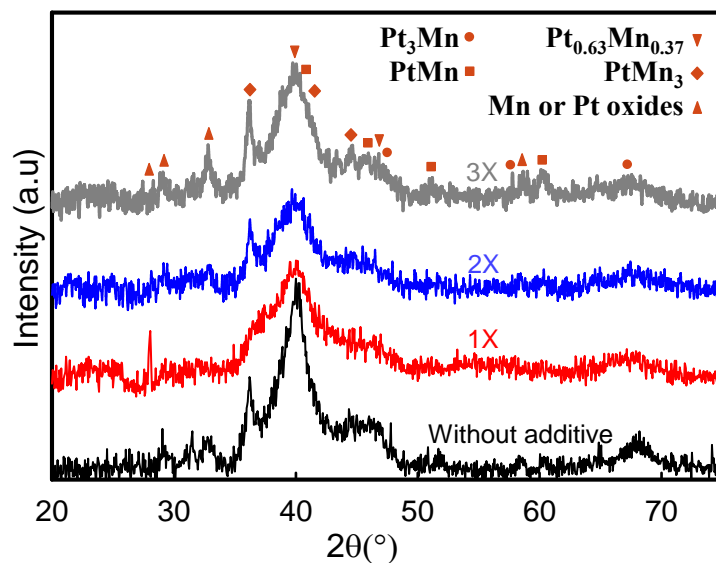


**Figure 3.** XRD analysis of the samples, which were prepared in the presence and absence of sodium citrate.

The XRD patterns obtained for Pt-Mn catalysts prepared with 2X SC that were heat treated at different temperatures are presented in Figure 4. As has been shown previously [10], heat treatment has a great impact on the activity and the crystallite structure of the Pt-Mn samples produced without the additive. Here, we have observed similar results for the samples prepared in the presence of SC. The peak at  $36.2^\circ$  associated with the Mn-rich phases in the XRD pattern disappeared after heat treatment at  $500^\circ\text{C}$  for 1 h and the intensity of the remaining peaks increased with crystallization. However, the predominant structure was still the Pt face-centered cubic (fcc) structure.

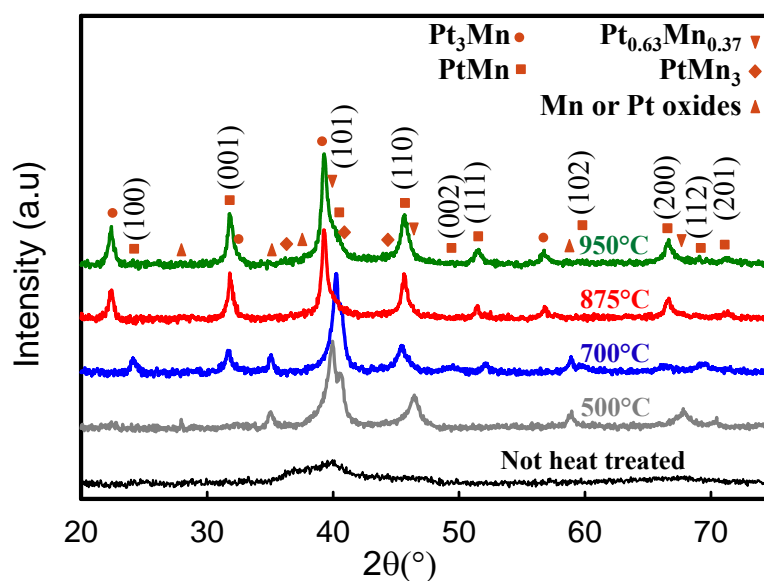


**Figure 4.** The XRD patterns of the sample prepared in the presence 2X SC and after heat treatment at different temperatures.

Upon further increasing the heat treatment temperature to 700 °C, substantial changes were observed. New peaks at lower diffraction angles (22°–40°) indicate that the ordered Pt-Mn intermetallic phase was formed at 700 °C. The Pt-Mn intermetallic phase [34] has a tetragonal structure; therefore, new peaks, (001) and (100), were demonstrated at lower diffraction angles of ~24.1° and ~37.1°, respectively. As a result of Pt and Mn further alloying and intermetallic phase formation, the peak shifts from 39.8° up to 40.2° and 46.5° down to 45.5° were observed when heat treatment temperature increased from 500 up to 700 °C. The shift and the intensity decline of the peaks at 39.8° and 46.5° can be assigned to the completion of phase modifications at 700 °C [10]. In Figure 5, the XRD spectra of samples prepared in the presence of SC and heat treated at 700 °C for different periods are compared. The spectra show that the phase transformation was completed after 1 h of heat treatment, and further increasing of the heat treatment time has no effect on the structure of the samples. The optimum heat treatment period for the samples prepared without SC was 4 h [10]. Presumably, smaller particle sizes undergo a faster phase transformation, which has also been found by the TGA and DSC analysis. This fast phase transformation is very beneficial, since a shorter treatment time should minimize particle size growth, yielding a higher active surface area and potentially improved electrochemical activity.

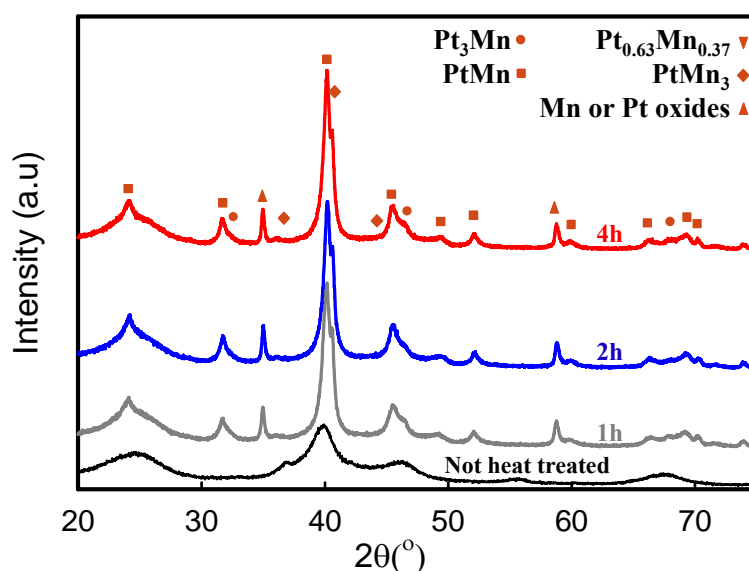
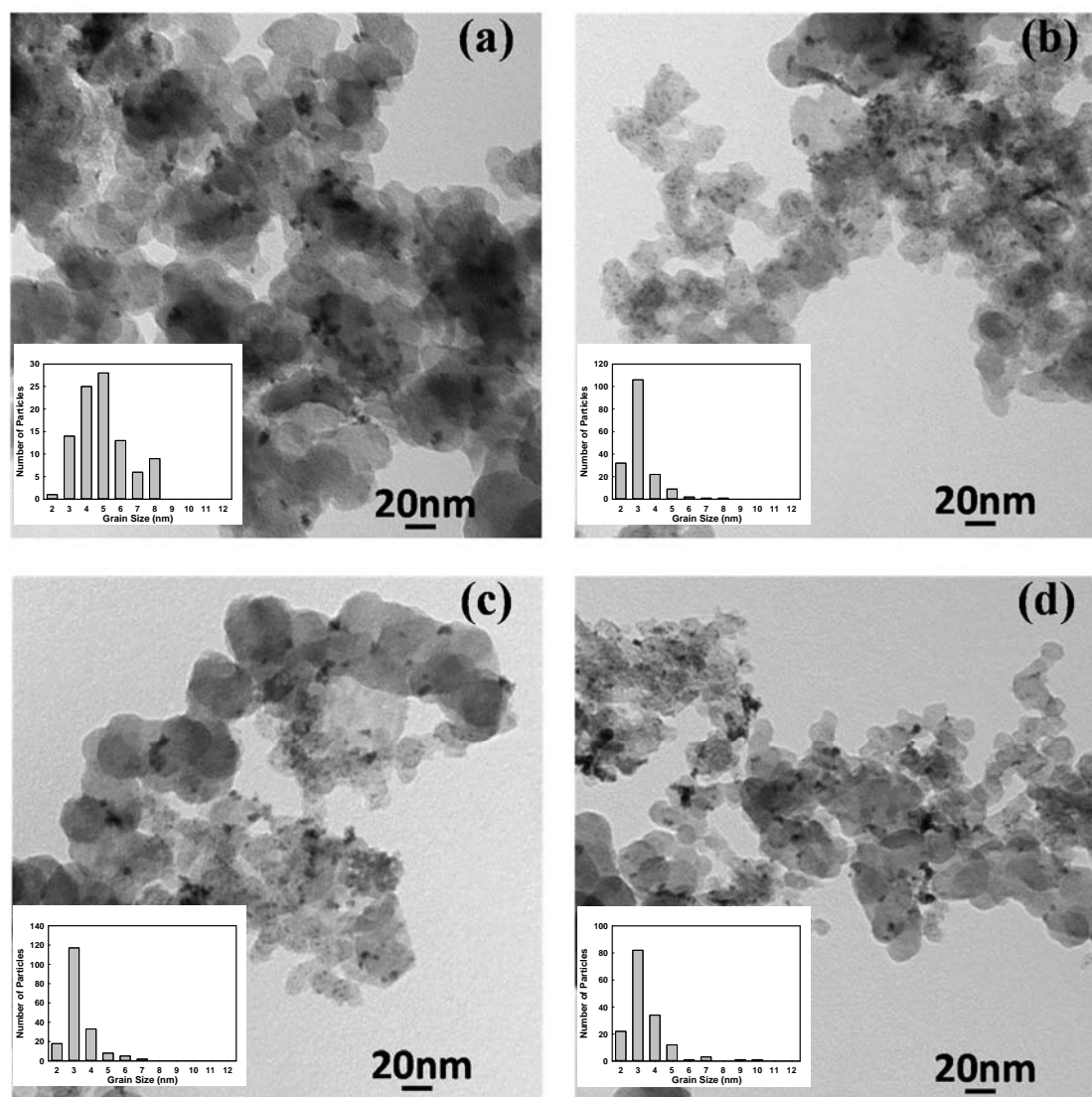


**Figure 5.** The XRD patterns of the sample prepared in the presence of 2X sodium citrate (SC) and after heat treatment at 700 °C for different periods.

In Figure 4, when the heat treatment temperature increased to 875 °C and 950 °C, additional peaks at 22.4° and 39.4° were observed. This variation in the crystalline structure of the Pt-Mn samples is due to a phase separation and the formation of phases with higher Pt content, such as Pt<sub>3</sub>Mn. This phenomenon is also observed for the Pt-Mn samples prepared without SC [10].

TEM images of as-synthesized samples with and without the additive are presented in Figure 6. The mean particle sizes measured by using the TEM images are given in Table 1. These TEM images showed that the catalysts with nanosized metal particles were synthesized, and adding sodium citrate dramatically decreased the particle sizes and reduced the agglomeration of alloy particles. Correspondingly, the particle dispersion was improved in the presence of sodium citrate. However, increasing the sodium citrate ratio to 3X amplified the agglomeration and deteriorated the particle

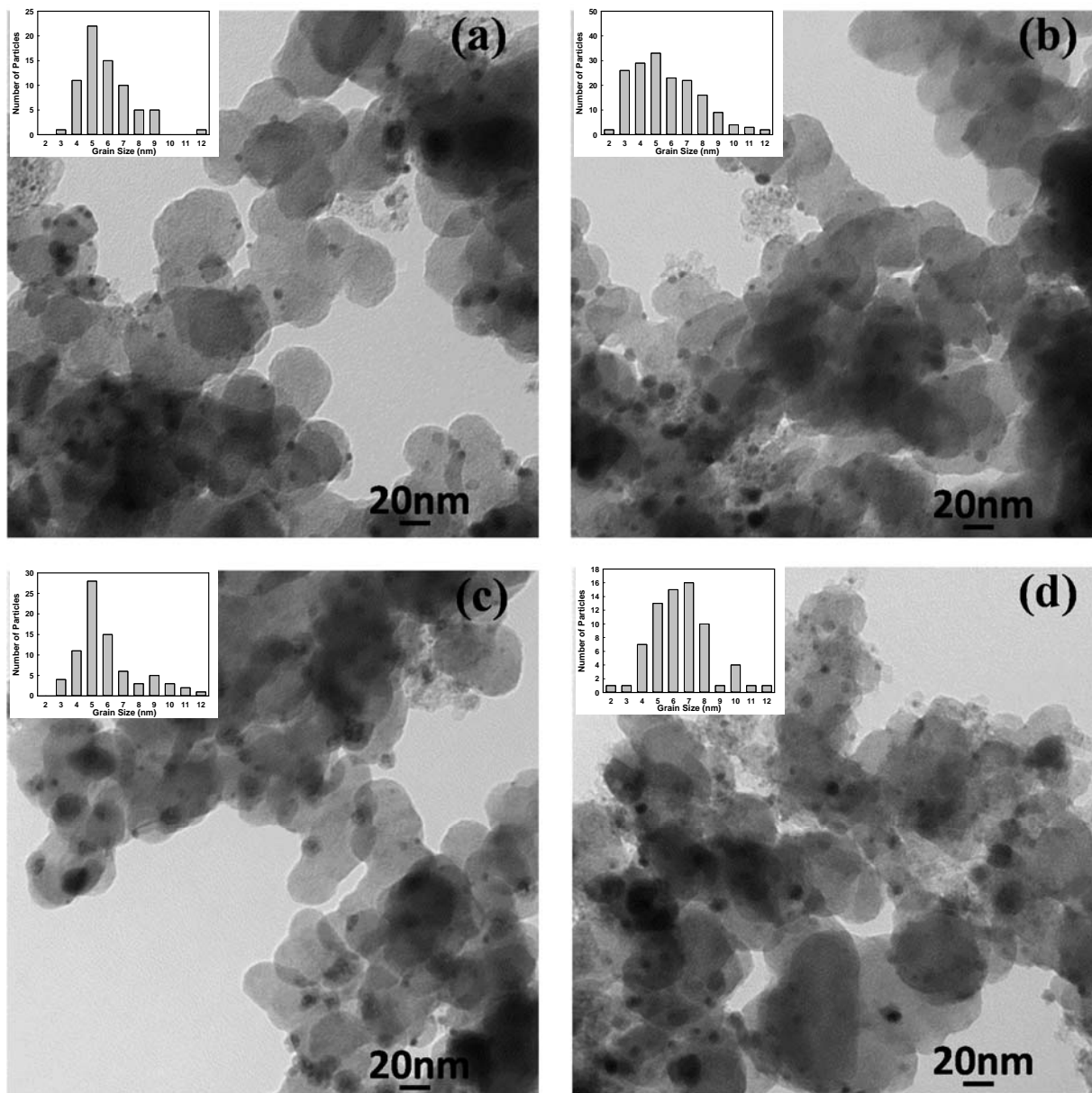
dispersion. It seems that adding further sodium citrate blocked the particle nucleation sites on the surface of carbon black particles, which directed the metal particle deposition toward the grain boundaries of carbon black particles. Therefore, the metal particle agglomeration was observed in between carbon particles. Furthermore, TEM images once more proved that smaller particle sizes and better particle dispersion in the presence of SC were responsible for facilitating the phase transformation during heat treatment and changing the start temperature of thermally-activated processes, which were observed in the TGA and DSC analyses.



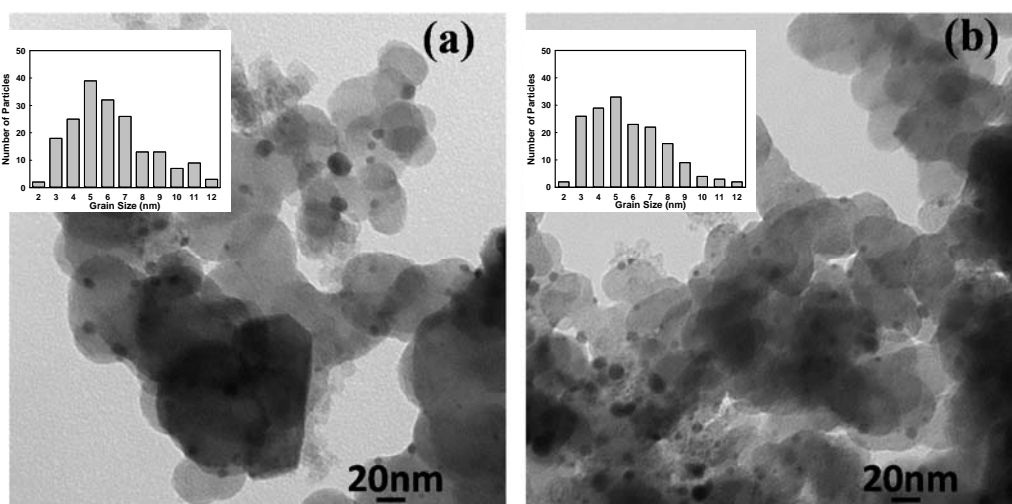
**Figure 6.** TEM image of Pt<sub>0.75</sub>Mn<sub>0.25</sub> samples prepared in the presence of different contents of sodium citrate: (a) no additive; (b) 1X; (c) 2X; and (d) 3X.

Figure 7 displays TEM images of samples synthesized in the presence of SC that were heat treated at different temperatures. The particle sizes and details calculated from the TEM images are summarized in Table 1. The heat treatment increased the particle sizes, including some very large particles with a radius of more than 10 nm. However, the average particle size was enlarged by only 3 nm by increasing the heat treatment temperature to 950 °C. This means that Pt-Mn alloys were resistant to particle growth, which has also been observed for other alloys [35] and Pt-Mn samples produced without SC [10].

In Figure 8, the TEM images of two samples, which were prepared with and without SC and heat treated for 1 h at 700 °C, are compared. It can be concluded that the presence of SC improved the alloy particle dispersion and prevented the particle enlargement to a great extent during heat treatment. Therefore, it is expected that samples prepared with SC should show enhanced activity compared to samples prepared without additives or heat treated for a longer time.



**Figure 7.** TEM image of Pt<sub>0.75</sub>Mn<sub>0.25</sub> samples prepared in the presence 2X of sodium citrate and after heat treatment at different temperatures: (a) 500 °C; (b) 700 °C; (c) 875 °C; and (d) 950 °C.



**Figure 8.** TEM images of Pt<sub>0.75</sub>Mn<sub>0.25</sub> samples prepared (a) without additive and (b) in the presence 2X of sodium citrate and heat treated at 700 °C for 1 h.

## 2.2. Electrochemical Characterization

The results of electrochemical studies for Pt-Mn samples prepared with and without SC are presented in Figure 9a. The experiments were conducted in the deaerated 0.5 M H<sub>2</sub>SO<sub>4</sub> solution. The common Pt cyclic voltammetry (CV) shape with hydrogen adsorption/desorption peaks at lower potentials was observed for all samples. The electrochemical active surface area (ECSA) was calculated by integrating the charge under the hydrogen adsorption peaks and is compiled in Table 3 and Figure 10. The results show that the ECSA values were dramatically increased by adding SC from 10.5–20.6 m<sup>2</sup>/g<sub>Pt</sub> (Figure 10), which is in good agreement with the TEM and XRD results. The ECSA improvement is attributed to the superior particle dispersion and smaller grain sizes in the samples prepared with SC. The maximum ECSA value was achieved with the sample prepared using the 2X SC content. When the amount of SC was increased to 3X, the measured ECSA was lower than that measured for 2X. Based on the TEM analysis (Figure 5d), this reduced ECSA is the result of uneven particle dispersion on the carbon support.

CV obtained for samples prepared with 2X SC and heat treated at different temperatures is illustrated in Figure 9b. Heat treatment at 500 °C reduced the ECSA values for Pt-Mn samples, but the ECSA for the Pt-Mn samples improved after increasing the heat treatment temperature to above 700 °C. The ECSA values never reached the same value as the untreated sample. Particle size growth is the main cause of the drop in ECSA. However, the optimal ECSA was achieved after heat treatment at 700 °C for 1 h and led to an ECSA that was only 7% lower than that of the untreated sample. These results show that Pt-Mn samples prepared with SC are more resistant to particle growth compared to samples prepared without SC. Previously, it has been shown that the formation of the ordered structure and the generation of a higher alloying degree of Pt and Mn by changing the surface composition and structure enhanced the ECSA [10]. This resistance to ECSA loss is most likely due to a roughening of the alloy particle surface upon dissolution of the surface oxide layer [36] and also because of better particle dispersion and smaller grain sizes achieved in the presence of SC [37–39]. Additionally, the CV obtained with samples that were heat treated for different periods is shown in Figure 9c. Increasing the time of heat treatment to 4 h at 700 °C reduced the ECSA values (Table 3) (not shown in Figure 9c). A similar trend was also observed by increasing the heat treatment time at 500 °C.

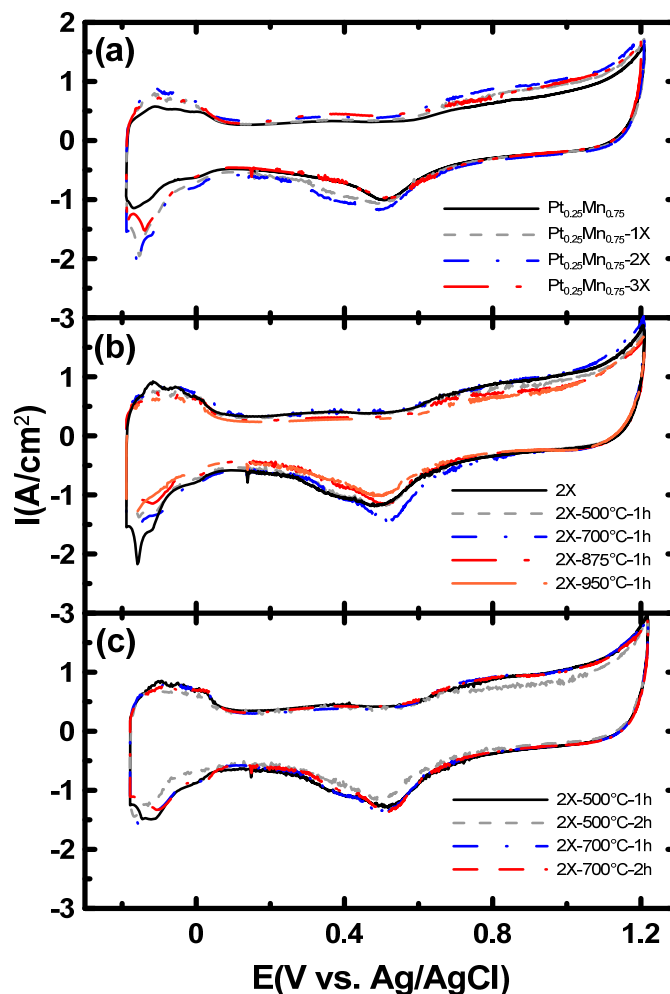


**Figure 9.** Cyclic voltammetry (CV) in the 0.5 M H<sub>2</sub>SO<sub>4</sub> solution at a scan rate of 20 mV/s for samples prepared (a) with different sodium citrate contents and then heat treated (b) at different temperatures for 1 h and (c) at 500 and 700 °C for different periods.

**Table 3.** Summary of ethanol oxidation reaction (EOR) activity parameters of the Pt-Mn samples. Also listed are the measured electrochemical active surface area (ECSA) values for each sample.

Samples	Onset potential (mV)	Current (mA·cm <sup>-2</sup> ) at 350 mV	Peak potential (mV)	Peak current (mA·cm <sup>-2</sup> )	ECSA (m <sup>2</sup> /g <sub>pt</sub> )
Pt <sub>0.25</sub> Mn <sub>0.75</sub>	248	0.461	665	2.49	10.5
Pt <sub>0.25</sub> Mn <sub>0.75</sub> -1x	247	0.472	678	2.72	16.8
Pt <sub>0.25</sub> Mn <sub>0.75</sub> -2x	249	0.489	690	2.81	20.6
Pt <sub>0.25</sub> Mn <sub>0.75</sub> -3x	266	0.355	695	2.14	15.7
Pt <sub>0.25</sub> Mn <sub>0.75</sub> -2X-500°C-1 h	248	0.880	703	6.49	16.2
Pt <sub>0.25</sub> Mn <sub>0.75</sub> -2X-700°C-1 h	240	0.628	710	8.40	19.1
Pt <sub>0.25</sub> Mn <sub>0.75</sub> -2X-875°C-1 h	237	0.602	729	4.50	17.1
Pt <sub>0.25</sub> Mn <sub>0.75</sub> -2X-950°C-1 h	233	0.638	703	4.76	14.5
Pt <sub>0.25</sub> Mn <sub>0.75</sub> -2X-500°C-2 h	245	0.655	662	4.58	13.8
Pt <sub>0.25</sub> Mn <sub>0.75</sub> -2X-500°C-4 h	241	0.709	671	3.87	15.4
Pt <sub>0.25</sub> Mn <sub>0.75</sub> -2X-700°C-2 h	240	0.588	682	6.30	17.1
Pt <sub>0.25</sub> Mn <sub>0.75</sub> -2X-700°C-4 h	241	0.556	698	6.35	15.7

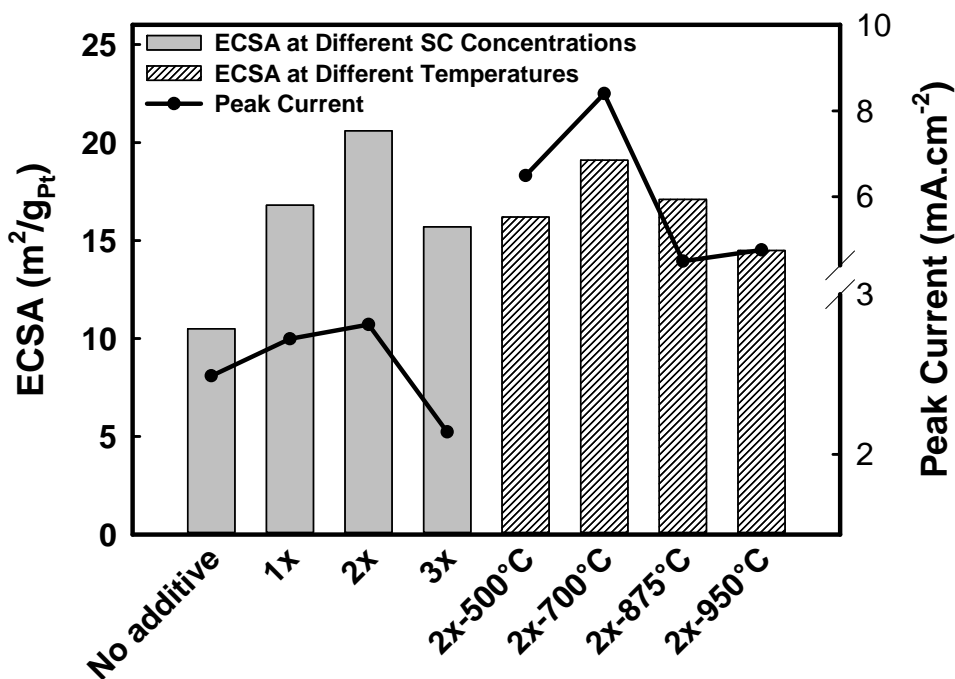


**Figure 10.** ECSA changes at different SC concentrations and after heat treatment at different temperatures, measured from Figure 9, and the ethanol oxidation peak current, measured from Figure 11.

The EOR activity of the samples prepared with and without sodium citrate is presented in Figure 11a. In addition, Pt/C, which was synthesized without SC, was also tested in ethanol solution and is referred to as Pt<sub>100</sub>. Comparing the electroactivity of the samples (Table 3 and Figure 10) showed that, by increasing the amount of sodium citrate to the 2X concentration, the activity of the samples was improved. The improvement in activity was a result of the higher ECSA and better particle dispersion, which was concluded from the TEM images and CV analysis in 0.5 M H<sub>2</sub>SO<sub>4</sub> solution. However, by increasing the amount of sodium citrate to 3X, the EOR activity was reduced. Based on XRD and TEM results, the lower electrochemical activity of samples prepared with 3X SC was related to the increase in the quantity of the oxide phase and, importantly, to uneven particle dispersion, which resulted in lower ECSA. Furthermore, the linear sweep voltammetry (LSV) in the ethanol solution showed that by adding SC, the onset potential of the samples was almost constant (247–249 mV) up to the optimum ratio (2X), but increased to 266 mV when higher ratios of SC were used.

The EOR activity of the samples after heat treatment is illustrated in Figure 11b. After performing the heat treatment at different temperatures, the activity was improved in all samples compared to the as-produced sample. The activity of heat-treated samples is reported in Table 3 and compared in Figure 10. The most active samples were produced at 700 °C, at which temperature the Pt-Mn ordered phase was formed. Upon increasing the heat treatment temperature to 850 and 950 °C, the EOR activity of the samples was decreased because of particle growth and forming new phases. However, the EOR activity of the heat-treated samples in all temperatures was greater than the untreated sample.

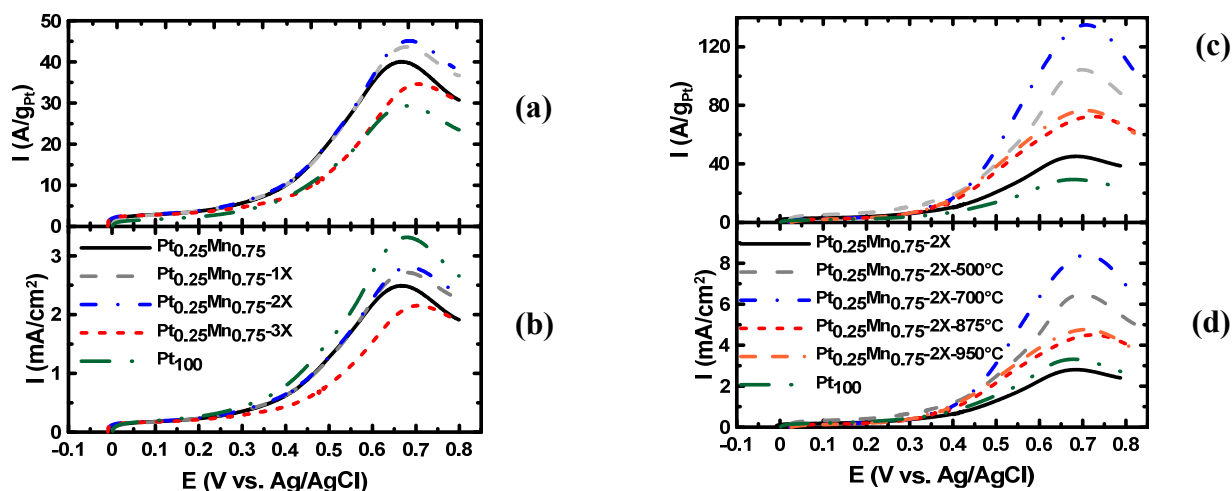


**Figure 11.** Linear sweep voltammetry (LSV) in the 0.5 M H<sub>2</sub>SO<sub>4</sub> + 0.1 M ethanol solution at a scan rate of 20 mV/s for: (a) the samples prepared with different sodium citrate contents; (c) the sample produced with 2X sodium citrate content and heat treated at different temperatures. (b) The same as (d), normalized for platinum content of (a) and (d), respectively.

The impact of heat treatment time at 500 °C and 700 °C on the EOR activity is shown in Figure 12. At 500 °C and 700 °C, increasing the heat treatment time beyond 1 h had a negligible impact on the EOR activity, which is in good agreement with the XRD and TGA results. The XRD patterns indicated that phase transformations occurred at 700 °C, and this does not change by increasing the time of heat treatment from 1 h to 4 h (Figure 5). Therefore, increasing the time of treatment can only affect the particle sizes, and as shown at 700 °C, the EOR activity slightly reduced by extending the time of the heat treatment.

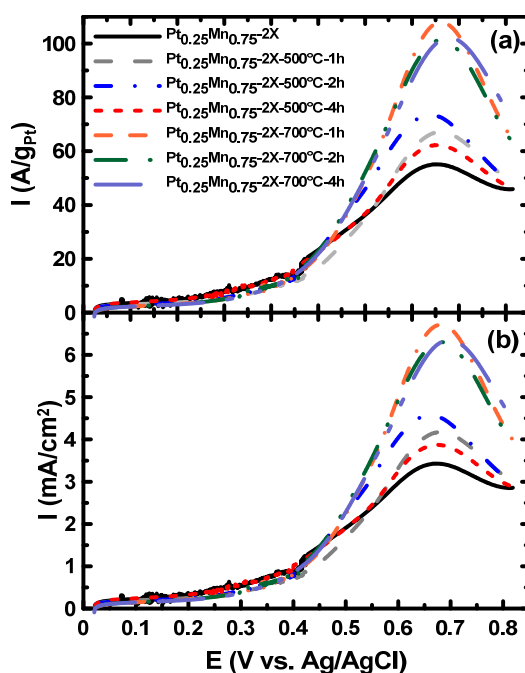


**Figure 12.** LSV of the samples prepared in the presence of sodium citrate and heat treated at 500 and 700 °C for different periods, in the 0.5 M H<sub>2</sub>SO<sub>4</sub> + 0.1 M ethanol solution at a scan rate of 20 mV/s.

### 3. Experimental Section

#### 3.1. Catalyst Synthesis

The impregnation method was used to prepare Pt-Mn/C catalysts with a composition of Pt<sub>0.25</sub>Mn<sub>0.75</sub>, similar to that previously published [4]. The metal precursors were H<sub>2</sub>PtCl<sub>6</sub>·H<sub>2</sub>O (Aldrich, Oakville, ON, Canada) and MnCl<sub>2</sub>·4H<sub>2</sub>O (Aldrich, Oakville, ON, Canada). Trisodium citrate (SC) (Aldrich) and Vulcan XC72R carbon black (Cabot Corp., Billerica, MA, USA) were used as an additive and metal support, respectively. The total metal loading was kept constant at ~20 wt. % for all samples. The SC was added in a weight ratio of 1:1, 2:1 and 3:1 to the metal ratios, which are represented in this article by 1X, 2X and 3X, respectively. The pH of the solution was adjusted using a HCl solution (15 v/v %) and/or a 1 M NaOH solution. NaBH<sub>4</sub> powder was used as the reduction agent. The weight ratio of NaBH<sub>4</sub> to the metal content was 3:1. In addition, a control sample of 20 wt. % Pt/C was synthesized with the same method without SC, which was referred to as Pt<sub>100</sub>. The powders were collected by suction filtration, washed with isopropanol alcohol (IPA), acetone and deionized water and, finally, dried in an oven at 80 °C overnight.

Heat treatment was performed in a nitrogen atmosphere at either 500, 700, 875 or 950 °C in a Barnstead Thermolyne tube furnace with a quartz tube. The period of heat treatment was kept constant (1 h) for all samples and temperatures, unless otherwise specified. After the heat treatment, the samples were cooled down under a constant flow of nitrogen gas and were preserved inside the furnace until room temperature was reached.

#### 3.2. Materials Characterization

The chemical composition of the Pt-Mn samples was examined by inductively-coupled plasma optical emission spectroscopy (ICP-OES, Varian Vista-MPX, Mississauga, ON, Canada). Aqua Regia solution was used to dissolve metal powders, and diluted solutions were consumed for ICP-OES analyses. ICP-OES instrument was calibrated by four standard solutions of Pt and Mn with concentrations of 1, 5, 10 and 20 ppm.

The carbon/metal weight ratio and the temperature of phase changes were determined by thermogravimetric analysis (TGA) and differential scanning calorimetry (DSC). Thermal analysis was performed using a TA Instruments Q600 SDT system (TA Instruments, New Castle, DE, USA). Measurements were made in both argon and air atmospheres, using a heating ramp of 5 °C/min and 20 °C/min, respectively.

Powder X-ray diffraction (XRD) patterns were obtained for each catalyst. Measurements were made using either a Bruker D8 Advance powder X-ray diffractometer (Bruker, East Milton, ON, Canada) equipped with a germanium monochromator (provided by Bruker) or a Rigaku Ultima IV X-ray diffractometer (Rigaku, Toronto, ON, Canada) equipped with a graphite monochromator (provided by Rigaku). Both instruments employ a Cu K<sub>α1</sub> X-ray source.

A Philips CM 10 instrument equipped with an AMT digital camera system was used for transmission electron microscopy (TEM, Philips, Andover, MA, USA) analysis. Samples for TEM analysis were dispersed in a mixture of water and isopropanol and applied to nickel 400 mesh reinforced grids coated by carbon and allowed to dry under air before being introduced into the chamber. The mean particle sizes were determined by measuring the diameter of 100–200 metal particles.

### 3.3. Electrochemical Characterization

The electrochemical activity of the samples was studied after applying a thin layer of catalyst on glassy carbon (GC) electrodes. The ink of samples was produced by mixing 10 mg of catalyst with 100  $\mu\text{L}$  Nafion solution (5% in alcohols, Dupont) and a 400  $\mu\text{L}$  50:50 mixture of isopropyl alcohol and water. A uniform suspension was achieved after sonicating for 45 min. A 2- $\mu\text{L}$  droplet of the well-dispersed catalyst ink was deposited onto a clean and polished GC electrode (diameter = 3 mm, CH instruments) and dried in air at room temperature prior to electrochemical tests. The total metal loading of the catalyst layer was 0.11 mg/cm<sup>2</sup>. Cyclic voltammetry (CV) and linear sweep voltammetry (LSV) were performed in a N<sub>2</sub>-purged solution. A 0.5 M H<sub>2</sub>SO<sub>4</sub> solution was used to determine the electrochemical active surface area (ESCA). A 0.5 M H<sub>2</sub>SO<sub>4</sub> + 0.1 M ethanol solution was employed to study the EOR activity of the catalysts. Measurements were made in a 3-electrode cell with a Pt wire counter electrode and a Ag/AgCl reference electrode. The LSV and CV for all samples were collected at a scan rate of 20 mV/s. Besides, the sample surfaces were cleaned prior to recording the final electrochemical test, by scanning at a scan rate of 100 mV/s and then at the scan rate of 20 mV/s, until we got a clean and reproducible CV.

## 4. Conclusions

This work has shown how the addition of sodium citrate (SC) influences the particle dispersion and grain size of Pt-Mn particles and facilitates the crystalline phase transformation. The results indicated that adding SC to the impregnation solution improved particle dispersion, decreased particle sizes, reduced the heat treatment time from 4 h to 1 h and increased the ECSA. Therefore, the EOR activity of the Pt-Mn alloy catalysts was enhanced. However, the weight ratio of SC to metal loading should be kept lower than 2X, because a higher weight ratio hindered the metal particle dispersion. Furthermore, this investigation proved that the SC had a positive impact on the EOR activity of Pt-Mn alloys when the pH of the impregnation solution was lower than four. Moreover, the heat-treated samples showed superior activity toward ethanol oxidation in comparison with the as-synthesized samples. The EOR activity was the highest for the sample heat treated at 700 °C for 1 h. The XRD analysis illustrated that Pt-Mn intermetallic was formed at the same temperature, and this was the main reason for the superior activity.

## Acknowledgments

This work was supported by the Natural Sciences and Engineering Research Council (NSERC) of Canada and University of Ontario Institute of Technology (UOIT). The authors also acknowledge equipment support from the Canada Foundation for Innovation. We thank Wen He Gong (McMaster University) for the XRD data and Richard B. Gardiner (University of Western Ontario) for the TEM images.

## Author Contributions

M.R.Z.G. and E.B.E. conceived of and designed the experiment. M.R.Z.G. performed the experiment and primary data analysis. E.B.E. contributed reagents/materials/analysis tools. M.R.Z.G. and E.B.E. wrote the paper.

## Conflicts of Interest

The authors declare no conflict of interest. The founding sponsors had no role in the design of the study; in the collection, analyses or interpretation of data; in the writing of the manuscript; nor in the decision to publish the results.

## References

1. Antolini, E. Formation of carbon-supported PtM alloys for low temperature fuel cells: A review *Mater. Chem. Phys.* **2003**, *78*, 563–573.
2. Watanabe, A.; Uchida, H. Catalysts for the Electro-Oxidation of Small Molecules. In *Handbook of Fuel Cells—Fundamentals, Technology and Applications*; Vielstich, W., Lamm, A., Gasteiger, H., Eds.; John Wiley & Sons, Ltd.: Chichester, UK, 2010.
3. Liu, H.; Song, C.; Zhang, L.; Zhang, J.; Wang, H.; Wilkinson, D.P. A review of anode catalysis in the direct methanol fuel cell. *J. Power Sources* **2006**, *155*, 95–110.
4. Ammam, M.; Prest, L.E.; Pauric, A.D.; Easton, E.B. Synthesis, Characterization and Catalytic Activity of Binary PtMn/C Alloy Catalysts towards Ethanol Oxidation. *J. Electrochem. Soc.* **2012**, *159*, B195–B200.
5. Castro Luna, A.M.; Camara, G.A.; Paganin, V.A.; Ticianelli, E.A.; Gonzalez, E.R. Effect of thermal treatment on the performance of CO-tolerant anodes for polymer electrolyte fuel cells. *Electrochem. Commun.* **2000**, *2*, 222–225.
6. Cherstiouk, O.V.; Gavrilov, A.N.; Plyasova, L.M.; Molina, I.Y.; Tsirlina, G.A.; Savinova, E.R. Influence of structural defects on the electrocatalytic activity of platinum. *J. Solid State Electrochem.* **2008**, *12*, 497–509.
7. Vigier, F.; Rousseau, S.; Coutanceau, C.; Leger, J.; Lamy, C. Electrocatalysis for the direct alcohol fuel cell. *Topics Catal.* **2006**, *40*, 111–121.
8. Ammam, M.; Easton, E.B. Ternary PtMnX/C (X = Fe, Co, Ni, Cu, Mo and, Sn) Alloy Catalysts for Ethanol Electrooxidation. *J. Electrochem. Soc.* **2012**, *159*, B635–B640.
9. Ammam, M.; Easton, E.B. Quaternary PtMnCuX/C (X = Fe, Co, Ni, and Sn) and PtMnMoX/C (X = Fe, Co, Ni, Cu and Sn) alloys catalysts: Synthesis, characterization and activity towards ethanol electrooxidation. *J. Power Sources* **2012**, *215*, 188–198.
10. Zamanzad Ghavidel, M.R.; Easton, E.B. Thermally induced changes in the structure and ethanol oxidation activity of Pt<sub>0.25</sub>Mn<sub>0.75</sub>/C. *Appl. Catal. B* **2015**, *176-177*, 150–159.
11. Bezerra, C.W.B.; Zhang, L.; Liu, H.; Lee, K.; Marques, A.A.L.B.; Marques, E.P.; Wang, H.; Zhang, J. A review of heat-treatment effects on activity and stability of PEM fuel cell catalysts for oxygen reduction reaction. *J. Power Sources* **2007**, *173*, 891–908.
12. Lee, K.; Zhang, J.; Wang, H.; Wilkinson, D.P. Progress in the synthesis of carbon nanotube- and nanofiber-supported Pt electrocatalysts for PEM fuel cell catalysis. *J. Appl. Electrochem.* **2006**, *36*, 507–522.
13. Liu, Z.; Lee, J.Y.; Chen, W.; Han, M.; Gan, L.M. Physical and Electrochemical Characterizations of Microwave-Assisted Polyol Preparation of Carbon-Supported PtRu Nanoparticles. *Langmuir* **2003**, *20*, 181–187.

14. Bonnemann, H.; Richards, R.-M. Nanoscopic Metal Particles- Synthetic Methods and Potential Applications. *Eur. J. Inorg. Chem.* **2001**, *2001*, 2455–2480.
15. Xiong, L.; Manthiram, A. Nanostructured Pt-M/C (M = Fe and Co) catalysts prepared by a microemulsion method for oxygen reduction in proton exchange membrane fuel cells. *Electrochim. Acta* **2005**, *50*, 2323–2329.
16. Antonucci, P.L.; Alderucci, V.; Giordano, N.; Cocke, D.L.; Kim, H. On the role of surface functional groups in Pt carbon interaction. *J. Appl. Electrochem.* **1994**, *24*, 58–65.
17. Hui, C.L.; Li, X.G.; Hsing, I.M. Well-dispersed surfactant-stabilized Pt/C nanocatalysts for fuel cell application: Dispersion control and surfactant removal. *Electrochim. Acta* **2005**, *51*, 711–719.
18. Moghaddam, R.B.; Pickup, P.G. Support effects on the oxidation of ethanol at Pt nanoparticles. *Electrochim. Acta* **2012**, *65*, 210–215.
19. Tian, J.H.; Wang, F.B.; Shan, Z.H.Q.; Wang, R.J.; Zhang, J.Y. Effect of Preparation Conditions of Pt/C Catalysts on Oxygen Electrode Performance in Proton Exchange Membrane Fuel Cells. *J. Appl. Electrochem.* **2004**, *34*, 461–467.
20. Di Noto, V.; Negro, E. Pt-Fe and Pt-Ni Carbon Nitride-Based “Core-Shell” ORR Electrocatalysts for Polymer Electrolyte Membrane Fuel Cells. *Fuel Cells* **2010**, *10*, 234–244.
21. Di Noto, V.; Negro, E. Development of nano-electrocatalysts based on carbon nitride supports for the ORR processes in PEM fuel cells. *Electrochim. Acta* **2010**, *55*, 7564–7574.
22. Easton, E.B.; Zamanzad Ghavidel, M.R.; Reid, O.R.; Ammam, M.; Prest, L.E. Limiting the Amount of Oxides in Pt-Mn Alloy Catalysts for Ethanol Oxidation. In Proceedings of the 223rd ECS Meeting, Toronto, ON, Canada, 12–16 May 2013; MA2013–01(39), p. 1366.
23. Wang, X.; Hsing, I.M. Surfactant stabilized Pt and Pt alloy electrocatalyst for polymer electrolyte fuel cells. *Electrochim. Acta* **2002**, *47*, 2981–2987.
24. Yang, J.; Lee, J.Y.; Too, H.P. Size effect in thiol and amine binding to small Pt nanoparticles. *Analytica. Chimica. Acta* **2006**, *571*, 206–210.
25. Gasteiger, H.A.; Kocha, S.S.; Sompalli, B.; Wagner, F.T. Activity benchmarks and requirements for Pt, Pt-alloy, and non-Pt oxygen reduction catalysts for PEMFCs. *Appl. Catal. B* **2005**, *56*, 9–35.
26. Zeng, J.; Yang, J.; Lee, J.Y.; Zhou, W. Preparation of Carbon-Supported Core-Shell Au-Pt Nanoparticles for Methanol Oxidation Reaction: The Promotional Effect of the Au Core. *J. Phys. Chem. B* **2006**, *110*, 24606–24611.
27. Liao, S.; Holmes, K.A.; Tsaprailis, H.; Birss, V.I. High Performance PtRuIr Catalysts Supported on Carbon Nanotubes for the Anodic Oxidation of Methanol. *J. Am. Chem. Soc.* **2006**, *128*, 3504–3505.
28. Zeng, J.; Lee, J.Y. Effects of preparation conditions on performance of carbon-supported nanosize Pt-Co catalysts for methanol electro-oxidation under acidic conditions. *J. Power Sources* **2005**, *140*, 268–273.
29. Kangasniemi, K.H.; Condit, D.A.; Jarvi, T.D. Characterization of Vulcan Electrochemically Oxidized under Simulated PEM Fuel Cell Conditions. *J. Electrochem. Soc.* **2004**, *151*, E125–E132.
30. Baturina, O.A.; Aubuchon, S.R.; Wynne, K.J. Thermal Stability in Air of Pt/C Catalysts and PEM Fuel Cell Catalyst Layers. *Chem. Mater.* **2006**, *18*, 1498–1504.
31. Stobbe, E.R.; de Boer, B.A.; Geus, J.W. The reduction and oxidation behaviour of manganese oxides. *Catal. Today* **1999**, *47*, 161–167.

32. Ji, C.X.; Ladwig, P.; Ott, R.; Yang, Y.; Yang, J.; Chang, Y.A.; Linville, E.; Gao, J.; Pant, B. An investigation of phase transformation behavior in sputter-deposited PtMn thin films. *JOM* **2006**, *58*, 50–54.
33. Easton, E.B.; Yang, R.; Bonakdarpour, A.; Dahn, J.R. Thermal Evolution of the Structure and Activity of Magnetron-Sputtered TM-C-N (TM = Fe, Co) Oxygen Reduction Catalysts. *Electrochem. Solid-State Lett.* **2007**, *10*, B6–B10.
34. Ghosh, T.; Leonard, B.M.; Zhou, Q.; DiSalvo, F.J. Pt Alloy and Intermetallic Phases with V, Cr, Mn, Ni, and Cu: Synthesis As Nanomaterials and Possible Applications As Fuel Cell Catalysts. *Chem. Mater.* **2010**, *22*, 2190–2202.
35. Antolini, E. Formation, microstructural characteristics and stability of carbon supported platinum catalysts for low temperature fuel cells. *J. Mater. Sci.* **2003**, *38*, 2995–3005.
36. Watanabe, M.; Tsurumi, K.; Mizukami, T.; Nakamura, T.; Stonehart, P. Activity and Stability of Ordered and Disordered Co-Pt Alloys for Phosphoric Acid Fuel Cells. *J. Electrochem. Soc.* **1994**, *141*, 2659–2668.
37. Harlow, J.E.; Stevens, D.A.; Sanderson, R.J.; Liu, G.C.K.; Lohstreter, L.B.; Vernstrom, G.D.; Atanasoski, R.T.; Debe, M.K.; Dahn, J.R. Structural Changes Induced by Mn Mobility in a Pt<sub>1-x</sub>Mn<sub>x</sub> Binary Composition-Spread Catalyst. *J. Electrochem. Soc.* **2012**, *159*, B670–B676.
38. Stevens, D.A.; Mehrotra, R.; Sanderson, R.J.; Vernstrom, G.D.; Atanasoski, R.T.; Debe, M.K.; Dahn, J.R. Dissolution of Ni from High Ni Content Pt<sub>1-x</sub>Ni<sub>x</sub> Alloys. *J. Electrochem. Soc.* **2011**, *158*, B905–B909.
39. Chen, C.; Kang, Y.; Huo, Z.; Zhu, Z.; Huang, W.; Xin, H. L.; Snyder, J.D.; Li, D.; Herron, J.A.; Mavrikakis, M.; Chi, M.; More, K.L.; Li, Y.; Markovic, N.M.; Somorjai, G.A.; Yang, P.; Stamenkovic, V.R. Highly Crystalline Multimetallic Nanoframes with Three-Dimensional Electrocatalytic Surfaces. *Science* **2014**, *343*, 1339–1343.

© 2015 by the authors; licensee MDPI, Basel, Switzerland. This article is an open access article distributed under the terms and conditions of the Creative Commons Attribution license (<http://creativecommons.org/licenses/by/4.0/>).